AIAA JOURNAL
Vol. 45, No. 4, April 2007

Design of a Fiber-Coupled Mid-Infrared Fuel Sensor for Pulse Detonation Engines

Adam E. Klingbeil,* Jay B. Jeffries,† and Ronald K. Hanson‡
Stanford University, Stanford, California 94305

DOI: 10.2514/1.26504

A mid-infrared laser absorption sensor is designed and used for time-resolved fuel concentration measurements in pulse detonation engines. A 3.39 μm helium–neon laser is fiber coupled to the engine, enabling optical absorption measurements for engine firing rates ranging from 5 to 40 Hz. Individual components (e.g., fiber-coupling lenses, optical fiber, and detectors) are optimized to minimize the effects of vibration and thermal emission. Fiber-coupling enables delicate components to be isolated from engine vibration and detonation pressure waves. The first-generation design is used to measure ethylene concentration with a single-cycle signal-to-noise ratio of ~7 for fired tests. The sensor is redesigned and measurements are performed on a different engine at multiple axial locations to extract fuel time of flight and concentration. Ethylene and propane concentration measurements were made, demonstrating the versatility of the sensor for multiple fuels. Single-cycle measurements of ethylene for fired tests have a signal-to-noise ratio of ~6 whereas measurements of propane have a signal-to-noise ratio of ~80, reflecting the larger absorption coefficient of propane at this wavelength. Comparison of fired and unfired tests reveals the effects of cycle-to-cycle interactions for the fired tests. Time-resolved fuel concentration measurements are shown to be crucial for understanding engine dynamics in high-repetition-rate pulse detonation engines.

Nomenclature

A_{detector}	=	detector area
a_{in}	=	spot size (1/e radius) of a beam that is being focused
a_{min}	=	diffraction-limited focused spot size (1/e radius)
D	=	fiber diameter
D_{Annulus}	=	annulus outer diameter
D_{Core}	=	inner diameter of annulus
D^*	=	detector responsivity
f	=	lens focal length
$(I/I_0)_\lambda$	=	fractional transmission at wavelength λ
L	=	path length, cm
N	=	number of transverse modes of a collimated beam
NA	=	numerical aperture of an optical fiber
P	=	total static pressure, atm
P_i	=	partial pressure of species i
P_{incident}	=	optical power incident on a detector
P''_{incident}	=	optical power per unit area incident on a detector
X_i	=	mole fraction of species i
α	=	absorbance
β_λ	=	absorption coefficient, $\text{cm}^{-1} \cdot \text{atm}^{-1}$
Δf	=	detector frequency bandwidth
$\Delta\alpha$	=	absorbance difference
λ	=	wavelength

I. Introduction

FUEL concentration measurements are critical for propulsion applications because stoichiometry affects pollutant emissions, power output, fuel efficiency, and engine stability. Additionally, research engines require accurate fuel diagnostics to improve understanding of the complex physical processes that govern the mixing and combustion of the fuel and oxidizer. One type of research engine, the pulse detonation engine (PDE), has recently received great attention in the aeropropulsion community because of its potential for increased thermodynamic efficiency and reduced mechanical complexity [1,2]. Simply stated, a PDE is a tube closed at one end and open at the other. The tube is filled with a fuel/air mixture that is ignited at the closed end. A combustion wave forms, starting out as a deflagration and quickly evolving into a detonation. As the detonation wave exits the open end of the tube, the exhaust gases exit the tube at high velocities, creating thrust. This cycle is repeated, to provide continuous thrust.

Whereas the most basic PDE is a simple device, it can be challenging to maintain stable and efficient engine operation at high firing rates. It has been shown that overall fuel stoichiometry and axial fuel distribution are both critical parameters for PDE operation [3]. Thus, accurate and time-resolved fuel diagnostics are needed to aid understanding of the effects of fuel loading and distribution on PDE operation at high repetition rates.

Optical absorption of near-infrared (near-IR) laser light has previously been used to study the time history of ethylene concentration in a PDE. That earlier work illustrated the usefulness of time-resolved fuel measurements to optimize and control fuel valve timing [4]. However, because the near-IR light probes the first overtone of the C–H vibrational stretching modes, the absorption coefficients are small. Larger hydrocarbon species (e.g., propane, jet fuel), have even smaller absorption coefficients in the near-IR, hence limiting usefulness of near-IR fuel sensing. Clearly, a more universal fuel sensor is needed for PDE research [5,6].

Mid-IR absorption at ~3.4 μm is approximately 100 times stronger than near-IR absorption because this mid-IR light accesses the fundamental frequencies of the C–H stretch while absorption in the near-IR accesses overtone frequencies. The 3.39 μm HeNe laser is an inexpensive mid-IR source that is well-suited for optical absorption measurements of hydrocarbons. This laser has been demonstrated for fuel detection in several practical devices including a gas turbine combustor [7], an internal combustion engine [8], and an unfired PDE [9,10].

We have designed a fiber-coupled mid-IR diagnostic using a 3.39 μm HeNe to measure time-resolved fuel concentration in a fired PDE. We demonstrate this sensor by measuring ethylene and propane concentrations in a PDE. The robust design of this sensor

Received 12 July 2006; accepted for publication 21 December 2006.

*Research Assistant, Department of Mechanical Engineering, 6061 Panama Mall. Student Member AIAA.
†Senior Research Engineer, Department of Mechanical Engineering, 6061 Panama Mall. Associate Fellow AIAA.
‡Professor, Department of Mechanical Engineering, 6061 Panama Mall. Fellow AIAA.

enables precise fuel concentration measurements, despite severe vibration of the PDE. This same sensor is applicable to many hydrocarbon fuels [11,12].

First, the optical engineering used to select the individual components of the sensor is described (i.e., the optical fiber, detector, and other optical components). The sensor layout is described for demonstration measurements in an ethylene-fueled PDE, where it is used to record fuel time of arrival and concentration. Improvements are then made to the sensor to reduce interference from thermal emission and the second-generation sensor is used to measure both ethylene and propane in a fired PDE. These measurements confirm that the sensor is robust, providing the capability to measure time-resolved fuel concentration in the harsh environments typical of ground test applications.

II. Fuel Sensor Design

We begin the discussion of fuel sensor design with a review of Beer's law of optical absorption, which relates fractional transmission of a monochromatic source to the concentration of an absorbing species. We then describe how single-mode and multimode beams are focused and collimated and how this affects the fiber selection. Subsequently, we discuss detector characteristics and the criteria that were used to choose our detector. Finally, we describe the detailed design of our first-generation fiber-coupled fuel sensor.

A. Optical Absorption by a Gaseous Mixture

Optical absorption is a line-of-sight technique that can be used to measure the mole fraction of a target species. Beer's law describes absorption of a monochromatic source, with wavelength λ, in a uniform gaseous mixture with a single absorbing species:

$$\left(\frac{I}{I_0}\right)_\lambda = \exp(-\beta_\lambda P X_i L) = \exp(-\beta_\lambda P_i L) \tag{1}$$

The quantity $\beta_\lambda P_i L$ is known as the absorbance and in this paper is given the symbol α. Measurements of the fractional transmission can be used to calculate mole fraction of the absorbing species if the total pressure, path length, and absorption coefficient are known.

In our measurements, the pressure is approximately atmospheric and the path length was measured. It should be noted that the absorption coefficient β_λ can be a function of pressure and temperature. For the fuels used in the present work (i.e., ethylene and propane), the pressure dependence can be neglected. However, temperature dependence must be considered. For the room-temperature measurements of propane, we used an absorption coefficient of 8.2 $\text{cm}^{-1} \cdot \text{atm}^{-1}$; for ethylene, the absorption coefficient was 0.193 $\text{cm}^{-1} \cdot \text{atm}^{-1}$ at room temperature and 0.2 $\text{cm}^{-1} \cdot \text{atm}^{-1}$ at 430 K. The small temperature dependence of the ethylene absorption coefficient simplifies the interpretation of the data for conditions with uncertainty in the gas temperature.

B. Design Considerations

When designing a fiber-coupled sensor for harsh environments, it is critical to optimize the individual components. The fuel sensor, schematically shown in Fig. 1, can be divided into three sections: 1) the fiber-coupling section, 2) the test section, and 3) the detection section. The HeNe laser is coupled into a fiber that routes the beam to the engine. The beam passes through the engine and is collected into the detection section and measured with a mid-IR detector. Here we discuss selection of the sensor components that need to be optimized, including fiber-coupling lenses, optical fiber, and mid-IR detectors.

The choice of optical fibers depends strongly on the minimum spot size of the beam. For a beam with a single Gaussian transverse mode, the diffraction-limited spot size (1/e radius), $a_{\min}$, is given by the following equation [13]:

$$a_{\min} = \frac{f\lambda}{\pi a_{\text{in}}} \tag{2}$$

Thus, a lens with a short focal length can be used to minimize the focused spot size. For a beam with a multiple number of transverse modes N, the focused spot size scales in proportion to $Nf\lambda/a_{\text{in}}$. For our sensor, we selected a plano-convex lens with 1 cm focal length, and for our multimode laser, the beam was focused from a measured spot size of $\sim$650 μm (1/e diameter $\sim$1.3 mm) to a spot size of $\sim$31 μm (1/e diameter $\sim$62 mm).

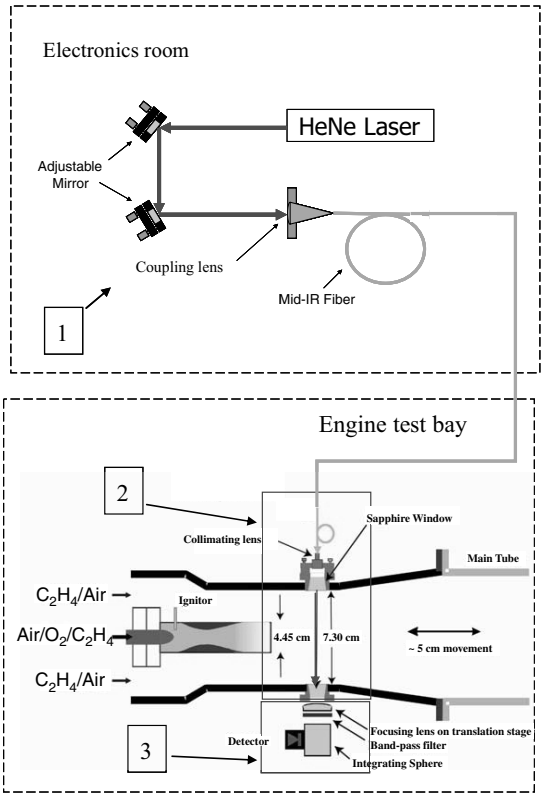

Fig. 1 Fuel sensor schematic: 1) fiber-coupling section, 2) test section, and 3) detection section.

The diameter of the optical fiber is also an important design parameter because it directly affects the ease and efficiency of coupling into the fiber as well as the quality of the beam exiting the fiber. Light is more easily coupled into a large-diameter fiber. However, large-diameter fibers support more transverse modes. A collimated beam with a large number of transverse modes suffers from greater divergence and has a larger focused spot size. Additionally, small movements of the fiber cause the energy in the individual modes to be redistributed randomly. The energy from each mode must be collected with equal efficiency or this redistribution will result in a phenomenon known as "mode noise." The number of transverse modes that can be propagated in a fiber is given by the following equation [14]:

$$N = 0.5\left(\frac{\pi D(\text{NA})}{\lambda}\right)^2 \tag{3}$$

Thus, to minimize the number of transverse modes, the fiber diameter and numerical aperture should be small. However, a large fiber diameter and numerical aperture enable easier optical alignment and less sensitivity to misalignment. For our sensor, we chose a 200-μm-diam fiber with numerical aperture of 0.27. This fiber diameter enabled easy coupling of our HeNe beam and allowed some misalignment between the laser, coupling lens, and fiber while maintaining a high coupling efficiency.

Optical fibers that transmit in the mid-IR are made from a variety of materials including fluoride glass, chalcogenide, sapphire, and silver halide. Sapphire fibers are unattractive for this application because they are expensive, brittle, and only available in short lengths (<2 m). Silver halide fibers are undesirable because they are expensive and their transmission properties are optimized for longer wavelengths ($\sim$6–14 μm). Chalcogenide and fluoride glass fibers

are both viable choices for this application. Fluoride glass fibers were selected because they are less expensive than chalcogenide fibers and provide lower reflection losses at the surfaces due to the lower refractive index of fluoride glass.

Like mid-IR optical fibers, mid-IR detectors use a variety of materials. These detectors can be divided into two main categories: 1) photo-voltaic (PV) and 2) photo-conductive (PC). A PV detector generates a current (or voltage) when light within the proper wavelength range is incident on it. In a PC detector, the electrical conductivity of the material is a function of the amount of light incident on it. PV detectors are preferred because PC detectors exhibit more "$1/f$ noise" where the detector noise is concentrated at low frequencies (i.e., the noise is not "white").

Having limited our selection to PV detectors, several choices are still possible including InSb, InAs, and HgCdTe detectors. An InSb detector is typically mounted in a large Dewar and requires cryogenic cooling, which makes it more difficult to mount to a vibrating PDE. InAs and HgCdTe detectors, however, are both available in compact, thermoelectrically cooled packages. In our testing, the HgCdTe detectors have exhibited spatially nonuniform response, making them more susceptible to mode noise and beam misalignment. Thus a thermoelectrically cooled InAs detector was chosen for our first-generation sensor.

Detectors are commonly characterized by a quantity known as the detectivity D^*, which is related to the noise equivalent power (NEP) through the following equation [15]:

$$D^* = \frac{\sqrt{A_{\text{detector}}\,\Delta f}}{\text{NEP}} \tag{4}$$

The NEP is the amount of incident power required to equal the magnitude of detector noise. Thus, the laser intensity signal-to-noise ratio (SNR) is given by

$$\text{SNR} = \frac{P_{\text{incident}}}{\text{NEP}} = \frac{P_{\text{incident}} D^*}{\sqrt{A_{\text{detector}}\,\Delta f}} \tag{5}$$

For our first-generation sensor, an integrating sphere was used to homogenize the light that was incident on the close-coupled detector. The effect was that the laser power exiting the integrating sphere was uniform across the sphere exit aperture, which was much larger than the detector element. In this case, the amount of light incident on the detector increases with detector area and the calculation of SNR changes to

$$\text{SNR} = \frac{P''_{\text{incident}} A_{\text{detector}}}{\text{NEP}} = \frac{P''_{\text{incident}} D * \sqrt{A_{\text{detector}}}}{\sqrt{\Delta f}} \tag{6}$$

[Note that if the integrating sphere exit aperture was smaller than the detector area, the incident power would be independent of the detector area and the SNR would be calculated by Eq. (5)]. Thus, the detector SNR is increased with large detectivity and detector area, but small frequency bandwidth. Our detector (Judson Technologies model J12-TE2-66D-R02M) was a two-stage thermoelectrically cooled InAs detector with a D^* of 4×10^{10} cm $\cdot$ Hz$^{1/2}$ $\cdot$ W^{-1} and a 2-mm-diam detection element. For the typical 30 μW of power incident on the detector and frequency bandwidth of 1 MHz, the SNR is $\sim$6600 and detector noise can be neglected for this measurement.

C. Fuel Sensor Design for a PDE

The fuel sensor system (Fig. 1) is composed of three components: 1) the fiber-coupling section, 2) the test section, and 3) the detection section. The fiber-coupling section is composed of the hardware and optics necessary to couple the 3.39 μm laser into the fiber and transmit the light to the engine. The test section is a modified engine section that provides optical access to the PDE. The optics and hardware that collect the transmitted beam from the test section and convert the light into a voltage signal are contained in the detection section. The design of each of these sections is described in more detail in the following paragraphs.

The first component of the fiber-coupling section is the 3.39 μm HeNe laser. The HeNe laser is a relatively inexpensive, widely available gas laser. Our laser is a Spectra-Physics model SP-124B HeNe laser with a power output of $\sim$5 mW at 3.39 μm and measured intensity noise of $\sim$0.3% (one standard deviation). We found that our laser emits laser light at both 3.39 μm and 1.15 μm. Whereas some of the 1.15 μm light was coupled into the fiber, an optical filter in the detection section removed the 1.15 μm light, leaving only the 3.39 μm component.

As a means of isolating the HeNe laser from the vibration of the engine, it was coupled into a fluoride glass fiber with core diameter of 200 μm, numerical aperture of 0.27, and length of 7 m (transmission = 80%@3.39 μm). The beam was reflected off two 1-in.-diam mirrors before being focused into the fiber. Each mirror was affixed to a 2-degree-of-freedom (DOF) rotating mount, allowing the beam to be precisely coupled into the small-diameter fiber. The beam was coupled into the fiber using a 6-mm-diam fused-silica plano-convex lens with a 8.7 mm nominal focal length (Avantes model Col-UV/Vis). The focused $1/e$ beam diameter with this lens is $\sim$62 μm, enabling efficient coupling of the beam with some latitude for misalignment and vibration. Although the fused-silica lens absorbs light at 3.39 μm, it is sufficiently thin to transmit $\sim$80% of the beam, including reflection losses at the lens surfaces. These lenses were preferred over standard IR lenses because they have a short focal length, they are mounted to fiber-coupling hardware, and the absorption losses are comparable to reflection losses of uncoated IR-grade optics.

In the test section, the light from the mid-IR fiber was collimated, and then transmitted across the diameter of the tube, through the test gas, and into the detection section. The beam was collimated using a second collimating lens (8.7 mm focal length). The collimating lens was rigidly attached to the engine, maintaining optical alignment as the engine was fired. Two tapered sapphire windows (1.25 cm clear aperture, 1.25 cm thickness) provided optical access to the engine. The taper was such that the pressure spikes behind the detonations forced the windows into the window mounts, insuring that the windows remained secure during engine operation.

From the test section the beam entered the detection section which was rigidly attached to the engine. In this section, the beam is first focused into an integrating sphere. The diffusely reflected light exits the integrating sphere, passes through a band-pass optical filter and onto the detector. The beam was focused into the integrating sphere using a sapphire plano-convex lens (2.54 cm diameter, 2.54 cm focal length). This lens was mounted in a 2-DOF X–Y translation stage so that the focal point of the lens could be precisely centered on the integrating sphere entrance aperture. The focused beam diameter at this point was $\sim$500 μm, which is sufficiently small to be easily coupled into the 6.35-mm-diam integrating sphere aperture. Between the detector and the integrating sphere, an optical band-pass filter (Spectrogon model NB-3390-060 nm) was used to reject thermal emission and the unwanted 1.15 μm radiation from the laser. The filter transmits $\sim$88% at 3.39 μm and has a 60 nm transmission band (FWHM) centered at 3.39 μm. The gold-coated integrating sphere has a 2.54 cm diameter and 6.35 mm ports (SphereOptics model SPH-1-4). Using this integrating sphere, only $\sim$2% of the light coupled into the sphere is incident on the detector. However, this sacrifice in power was acceptable because the integrating sphere renders the detection section insensitive to beam misalignment.

III. Fuel Measurements in a PDE

The first-generation fiber-coupled sensor was used to measure ethylene concentration in a high-repetition-rate PDE where the data were used to report fuel time of arrival and concentration. From these experiments, design changes were made to the sensor, leading to the second-generation fuel sensor. This sensor was subsequently used to measure ethylene and propane in a different PDE. Time-resolved fuel measurements in this latter engine revealed residual unburned fuel that could not be detected by standard ground testing instrumentation, but must be included in models of PDE

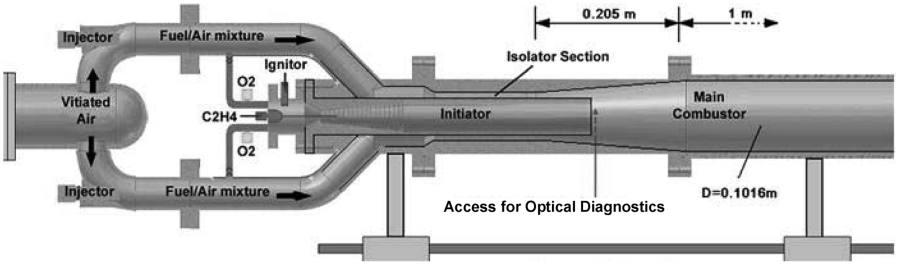

Fig. 2 Schematic of the PDE at the Naval Postgraduate School.

performance. Hence, the laser absorption diagnostic proved to be a valuable tool for optimizing engine performance and investigating cycle-to-cycle interactions.

A. PDE Description

A diagram of the air-breathing PDE is shown in Fig. 2 and is described in detail in [16]. The optical ports are located ∼2.5 cm downstream of the initiator exit. The engine is mounted on a thrust stand that allows it to travel ∼5 cm during a fired test, thus a free-space beam would not provide a useful measurement and fiber coupling is necessary.

Upstream of the test section, the engine is divided into two sections: an outer annulus and an inner core. An ethylene/air mixture flows through the outer annulus, and this mixture comprises ∼93% of the mass flow supplied to the engine. The ethylene/oxygen/air mixture in the inner core is responsible for initiating combustion and accelerating the transition from deflagration to detonation. The outer annulus of the engine (outer diameter = 7.3 cm, inner diameter= 4.45 cm) supplies a constant supply of vitiated air at ∼430 K (i.e., the air supply is valveless). Ethylene is injected into this airstream by four pulsed fuel injectors. Stoichiometry is controlled by the ethylene pressure supplied to these injectors. Air constantly flows through the initiator core (diameter = 4.45 cm) at a small flow rate. Before ignition, pulsed injectors in the initiator inject a small amount of ethylene and oxygen. The oxygen-enriched mixture in the initiator is then ignited with a spark plug, consuming the fuel/air mixture in the initiator and creating a combustion wave that passes into the main combustion chamber of the engine. For this engine design, the timing of the fuel injection relative to the ignition event is critical for detonation formation. Furthermore, control of overall stoichiometry and axial fuel distribution is crucial for efficient and stable operation. Thus, a time-resolved fuel diagnostic was anticipated to be a valuable tool for development of this PDE.

B. Fuel Measurements from the First-Generation Sensor

Ethylene concentration measurements were made for fired tests at repetition rates ranging from 10 to 40 Hz. Our measurements provided the time of arrival of the fuel as well as the fuel concentration. The temperature dependence of the ethylene absorption coefficient at the vitiator temperature of 430 K is small (∼5% change in β between 298 and 430 K) so that uncertainty in temperature of the vitiated air did not affect our measurements. The measured fuel concentration was then used to calibrate the main combustor stoichiometry as a function of the fuel supply pressure.

Single-cycle measurements for 40 Hz operation are shown in Fig. 3. Measurements made at other repetition rates yielded similar results that are not shown here. Data were plotted after 1 s of operation so that steady-state operation could be observed. The stages of the operating cycle for this PDE can be observed and an idealized fuel concentration profile is shown as a dashed line to aid interpretation of the data. The cycle begins when the fuel injector is commanded to open (i.e., at 1000, 1025, 1050 ms). At this point in the cycle, the main combustor has been purged, so there is no absorption of the beam. After ∼5 ms, the fuel arrives at the measurement location (1). Subsequently, the absorbance reaches an initial plateau value. At ∼12 ms into the cycle, a second increase of absorbance is observed due to arrival of the fuel injected in the initiator (2). A second plateau is observed, and then, after about 19 ms into the cycle, the detonation wave passes by the measurement station, consuming the fuel (3). For ∼5 ms following the detonation wave, broadband emission is detected, creating noise that appears as negative absorbance (4). However, the hot exhaust gases are quickly purged from the system, and the cycle begins again.

For the ethylene measurements, the absorption coefficient at 3.39 μm is low (0.19 $\text{cm}^{-1} \cdot \text{atm}^{-1}$ at 430 K), resulting in a peak absorbance of ∼0.10 for $X_{\text{ethylene}} = 7.2\%$. The dominant source of noise and measurement uncertainty results from the optical fiber vibrating while the engine is firing. While the fiber was constrained everywhere possible, the ∼0.7% intensity noise (for one standard deviation) from the vibrating optical fiber resulted in an absorbance SNR of ∼7 for the main combustor (i.e., the first plateau in Figs. 3 and 4) and a resultant measurement uncertainty of ∼14%. In comparison, before the first detonation event, the intensity noise was only 0.3%.

To improve the SNR of our measurement, we used a 10-cycle average of the measured absorbance, which reduced the measurement uncertainty to ∼5%. This enabled us to calculate accurate concentrations for the two observed plateaus in fuel concentration. Because our sensor was only one initiator diameter downstream of the initiator exit plane, the fuel/air mixtures from the core and annular regions were not fully mixed. Using the two plateau absorbance values from Fig. 4, the fuel concentration in the initiator and main combustor can be calculated using Eqs. (7) and (8):

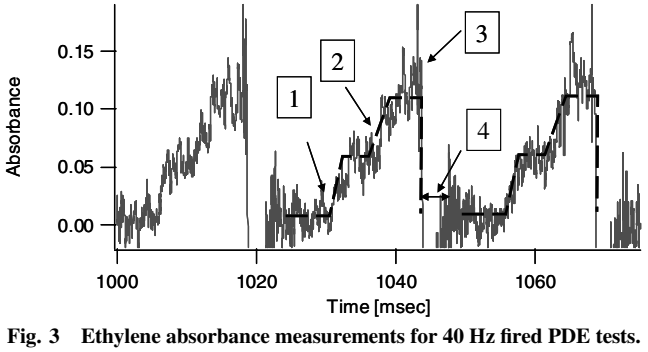

Fig. 3 Ethylene absorbance measurements for 40 Hz fired PDE tests.

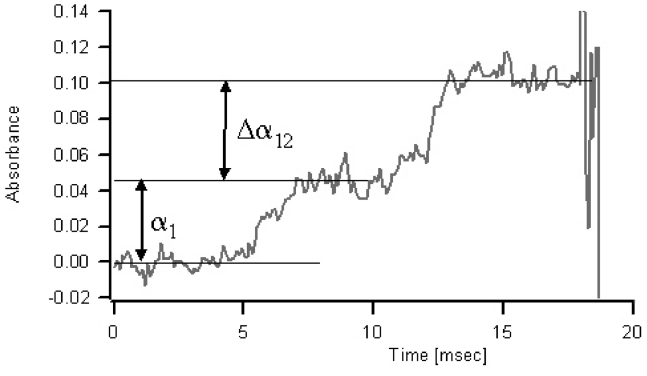

Fig. 4 Ten-cycle average of ethylene absorbance for 40 Hz fired PDE tests.

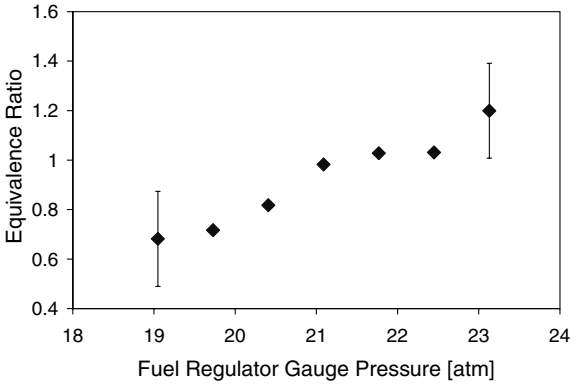

Fig. 5 Measured equivalence ratio for the main combustor vs ethylene regulator pressure.

$$X_{\text{MainCombustor}} = \frac{\alpha_1}{\beta_\lambda P(D_{\text{Annulus}} - D_{\text{Core}})} \tag{7}$$

Because the fuel entering the main combustor passes only through the annular section, the diameter of the core must be subtracted as it contains only air during the first fuel plateau. To calculate the fuel concentration in the initiator, the change in absorbance between the first and second plateaus is used:

$$X_{\text{Initiator}} = \frac{\Delta\alpha_{12}}{\beta_\lambda P D_{\text{Core}}} \tag{8}$$

The fuel mole fraction of the initiator was held constant at ~7.5% ($\phi = 1.2$) for our tests, while the stoichiometry of the main combustor was varied. The fuel sensor was then used to measure the dependence of the main combustor equivalence ratio on the ethylene pressure supplied to the fuel injectors, thereby calibrating the fuel injection system. The absorption sensor was used to calibrate the fuel/air stoichiometry as a function of fuel delivery pressure, as shown in Fig. 5. The error bars indicate one standard deviation of the measured equivalence ratio during the first plateau period and are an indication of the axial nonuniformity of the fuel concentration. Thus, the first generation of the mid-IR fuel sensor successfully captured the fuel time of arrival relative to the fuel injection timing and has enabled a stoichiometry calibration for the fuel system in the Naval Postgraduate School PDE. This calibration is useful for continued studies of engine performance, after the laser diagnostic has been removed from the engine.

C. Design Modifications for the Second-Generation Sensor

Testing of the first-generation mid-IR sensor revealed interferences from emission by the postcombustion gases and sensitivity to mechanical vibration of the optical fiber. The sensor was redesigned to reduce these effects and additional modifications were made to improve overall compactness and ease of installation. A schematic of the redesigned sensor is shown in Fig. 6. The fiber-coupling and detection sections are located in an electronics bunker whereas the test section is attached to the engine. In the redesigned sensor, a second optical fiber routed the beam back to an electronics bunker where the detection apparatus had been relocated. This modification isolated the detector from the engine vibration and allowed the use of a cryogenically cooled InSb detector. This detector provided better stability of the background signal and was more sensitive at our laser wavelength. Additionally, by replacing the large-aperture integrating sphere with a small-diameter optical fiber ($D \sim 480$ μm), we eliminated the thermal emission from the hot exhaust gases without exhibiting sensitivity to beam steering and misalignment.

In the redesigned sensor, a higher SNR was desired to eliminate the need for cycle averaging. One way to obtain a higher SNR would be to reduce the amount of noise contributed by fiber vibration. However, because fiber noise was comparable for all the fibers we tested and the fiber was already constrained from vibration as much as possible, no improvements were achieved in this regard. A second method to increase the SNR during the fuel-filling process is to use a combination of laser wavelength and fuel with a higher absorption coefficient. A significant increase in SNR was achieved when the fuel was changed from ethylene (absorption coefficient ~0.193 $\text{cm}^{-1} \cdot \text{atm}^{-1}$ at 298 K and 3.39 μm) to propane (absorption coefficient ~8.2 $\text{cm}^{-1} \cdot \text{atm}^{-1}$ at 298 K and 3.39 μm).

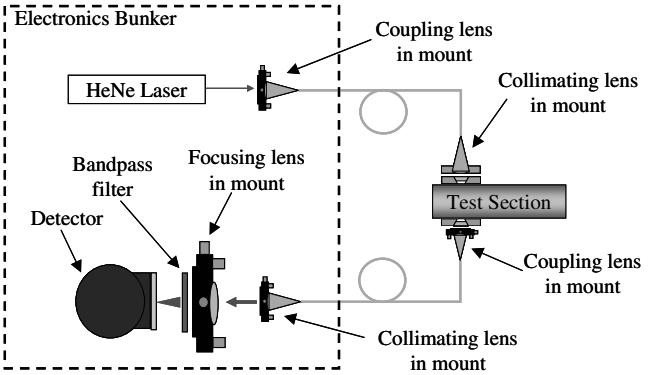

Fig. 6 Schematic of the second-generation fuel sensor for fuel measurements in a PDE.

The fiber-coupling optics were modified to reduce the spatial footprint of the sensor. Instead of using two adjustable mirrors, as in the previous design, the coupling lens was mounted in a 5-DOF translation/rotation mount. This single mount performed the task of the two adjustable mirrors and enabled sensitive alignment of the lens/fiber/laser combination while reducing the amount of space required by the sensor and reducing the amount of time required for alignment.

With the exception of the fiber-coupling scheme, all of the other optics and hardware for the fiber-coupling and test sections remained unchanged. However, several changes were made to the detection section. The beam was coupled from the test section into a second optical fiber (480 μm diameter, 2 m length), significantly reducing the amount of diffuse thermal radiation that was coupled into the detection section. This smaller aperture required a smaller focused spot size and more sensitive alignment than was previously implemented. To reduce the focused spot size, the 2.5 cm focal length lens was replaced with a 8.7 mm focal length lens, resulting in a focused spot size of ~200 μm compared to the ~500 μm spot size with the previous lens. The lens was mounted in a lockable 5-DOF translation/rotation stage so that the fiber-coupling optics could be easily aligned on the engine and bolted down during testing.

The fiber transmitted the beam to an adjacent electronics bunker, isolating the detector from the engine vibration and pressure waves. The beam exiting the optical fiber was collimated with another 8.7 mm focal length collimating lens, then focused onto a 2-mm-diam cryogenically cooled InSb detector (Judson Technologies model J10) using a sapphire plano-convex lens with a focal length of 2.5 cm and a resulting focused spot size of 640 μm. A band-pass filter (60 nm FWHM) was used to reject unwanted radiation.

D. Fuel Concentration Measurements with the Second-Generation Sensor

The second-generation sensor was demonstrated in an ethylene- and propane-fueled PDE. The engine, schematically shown in Fig. 7, has a 5 cm diameter and a total length of 147 cm. In the top configuration, the test section is located near the head of the engine. In the bottom configuration, the test section is located near the tail of the engine. The room-temperature air flows continuously while the fuel is valved. Measurements were made with the sensor located either 5 or 117 cm downstream of the igniter. For this engine, the fuel and air were combined into one tube upstream of the test section, resulting in a mixture that was more uniform than for the previous engine. Propane was measured for fired and unfired tests with a 5 Hz repetition rate. Although the absorption coefficient of propane is sensitive to temperature, the uncertainty in the room-temperature

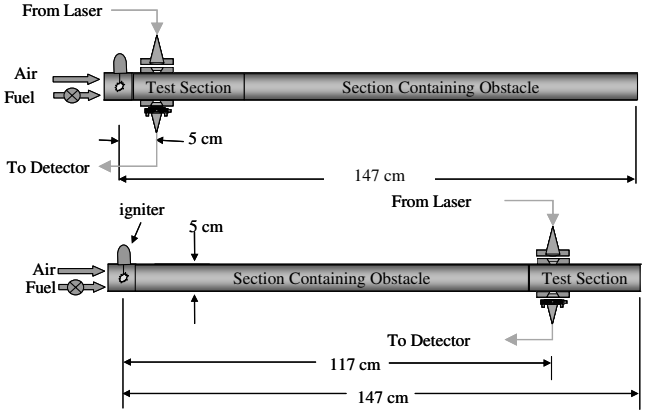

Fig. 7 PDE schematic for measurements made by the second-generation fuel sensor.

fuel/air mixture is small and concentration errors associated with this uncertainty are less than 1% of the measured concentration. Ethylene was measured for fired and unfired tests with firing rates between 5 and 20 Hz and with each experiment lasting 1 s. The sensor performance for 10 Hz engine operation is typical of performance at other frequencies. Measurements made at each of the two locations for equivalent operating conditions enabled calculation of bulk velocity of the test gas.

Single-cycle measurements had an SNR of ∼6. A nine-cycle average was used to improve the SNR of the measurement, resulting in an SNR of ∼17, with a corresponding measurement uncertainty of ∼6%. Each experiment lasted for 1 s (i.e., 10 cycles for 10 Hz operation), but the first cycle was not used in the ensemble because it did not reflect steady-state operation of the engine. Fuel partial pressure was calculated using Eq. (1) and the measured fractional transmission of our sensor. Sample measurements for 10 Hz operation are plotted in Fig. 8. The dashed line indicates a stoichiometric mixture of ethylene and air at 1 atm.

There are several things to note about these data. First, the time-of-flight between the two measurement locations is ∼20 ms, indicating a bulk velocity of ∼55 m/s. The bulk velocity can be used to calculate the amount of time required to partially or completely fill the engine with a fresh mixture. Knowledge of this filling time could allow optimization of the spark timing and enable characterization of engine performance as the amount of fresh mixture is varied.

Second, the detonation wave appears to arrive at the tail sensor before arriving at the head sensor. Because there was only one sensor, the measurements at the head and tail were obtained for different tests, but for identical operating conditions. Thus, the difference in time of arrival of the detonation wave is an artifact of the variability in detonation wave speed from test to test.

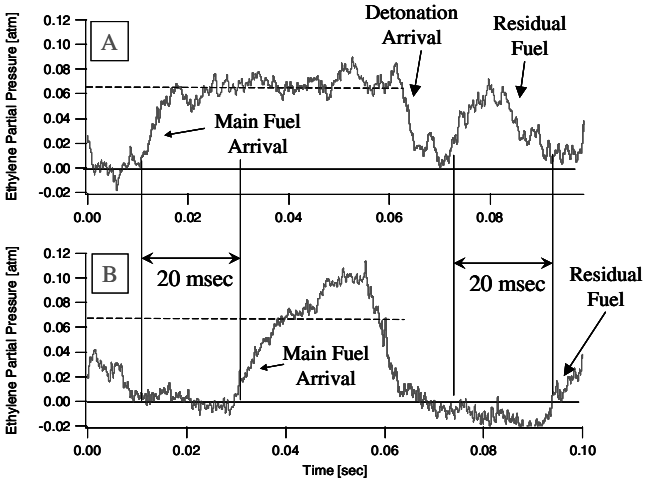

Fig. 8 Ethylene partial pressure measurements with the sensor located at a) the head end and b) the tail end.

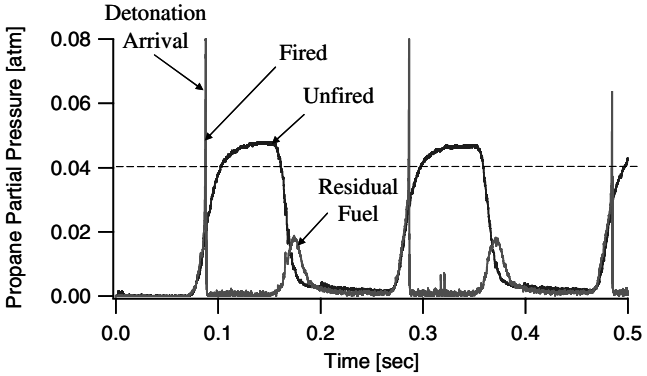

Fig. 9 Propane partial pressure measurements for 5 Hz fired and unfired tests.

Finally, after the detonation wave passes, a second burst of residual, unburned fuel is seen exiting the tube (note that this residual fuel appeared at the beginning of the subsequent cycle when the sensor was mounted at the tail of the engine and therefore appears as early fuel arrival). This residual fuel is a result of the pressure waves interacting with the fuel system, and it is desired that this fuel not be included in engine performance calculations. The standard fuel flow meters that are used in ground testing would not have identified this burst of unburned fuel, but our time-resolved diagnostic was capable of detecting the unburned pulse of fuel. Thus, the time-resolved fuel measurements have revealed some important flow dynamics and have enabled more accurate calculations of specific thrust, based on the amount of fuel that is actually burned in the engine and not on the total amount of fuel being supplied to the engine. This information is critical when comparing measured engine performance to PDE simulations [17] because specific thrust is inversely proportional to the amount of fuel used and accurate comparison to performance models requires that only the fuel burned inside the engine should be considered.

Experiments were also performed using propane as the fuel rather than ethylene. When compared to most hydrocarbon fuels, the absorption coefficient of ethylene at 3.39 μm is atypically small. Measurements of propane in a fired experiment illustrate how the sensor would perform for most other hydrocarbon fuels. The PDE was run at 5 Hz for both fired and unfired cases and the resulting fuel measurements are compared in Fig. 9. The dashed line indicates the partial pressure of propane required for a stoichiometric mixture at 1 atm. In the unfired tests, the propane partial pressure is shown to increase, reach a plateau, and then decrease after the fuel injection event has ended. In the fired tests, the propane partial pressure begins to increase, but before the plateau value is reached, the detonation wave passes and consumes the fuel. This indicates that the engine is underfilled. Because of the large absorption coefficient of propane, cycle averaging was not required to get an SNR of ∼80. The primary source of measurement uncertainty in this case is no longer the fiber noise. Instead, our uncertainty is dominated by the ∼3% uncertainty in absorption coefficient, which translates directly to uncertainty in fuel concentration.

From Fig. 9 we see that the mid-IR sensor exhibits a very high SNR for propane. Whereas the primary source of noise still comes from fiber movement, the absorption signal is significantly stronger, resulting in an improved SNR of ∼80. We also note that the residual burst of unburned fuel is observed for the fired case, but not the unfired case, confirming the role of postdetonation flow dynamics in producing the pulse of fuel.

Use of the fixed-wavelength 3.39 μm HeNe laser is attractive because it provides an inexpensive source for sensing hydrocarbons, but it lacks wavelength tunability. Fortunately, tunable mid-IR technology is currently becoming available that will enable wavelength optimization for any hydrocarbon fuel, including ethylene and propane [18]. The modular design of this sensor would allow the HeNe laser to be replaced with one of these tunable sources, resulting in even higher SNR through wavelength optimization.

IV. Conclusions

A mid-IR (3.39 μm) fiber-coupled sensor was developed to measure fuel concentration in fired pulse detonation engines. A compact and rugged design provided time-resolved fuel measurements for firing rates ranging from 5 to 40 Hz. The first-generation design provided fuel concentration and time-of-arrival data and enabled calibration of the pressure regulator that controls the fuel loading. This demonstration illustrates the potential of optical fuel sensing to improve ground test instrumentation.

An improved second-generation sensor eliminated the effects of background emission and also improved the ruggedness and compactness of the sensor. Fuel concentration and bulk velocity were obtained from the measurements in the second PDE. Single-cycle measurements of ethylene concentration had an SNR of $\sim$6 whereas measurements of propane had an SNR of $\sim$80. The improvement in SNR for propane is due to the larger absorption coefficient of propane. Our measurements revealed a residual burst of fuel that was present in the fired tests, but not in the unfired tests, illustrating that cycle-to-cycle interactions were causing some of the fuel to leave the engine unburned. It is crucial that these dynamic interactions be identified and characterized so that performance models can properly account for all of the fuel supplied to the engine. This discovery underscores the advantage of optical absorption diagnostics to provide time-resolved fuel concentration measurements during fired PDE tests. Furthermore, the simple, rugged design of our fiber-coupled sensor shows the potential for optical diagnostics in practical-scale test applications.

Acknowledgments

Support for the work done at the Naval Postgraduate School in Monterey, CA was provided by the ONR with Gabriel Roy as project manager and the AFOSR with Julian Tishkoff as project manager. Support for the research done at GE Global Research Center in Niskayuna, NY was provided by GE Global Research. We would like to acknowledge Chris Brophy and Jose Sinibaldi at the Naval Postgraduate School for providing access to the PDE used for our first-generation design. We would also like to acknowledge Kevin Hinckley and Anthony Dean at GE Global Research Center for providing PDE access for our second-generation sensor tests.

References

[1] Heiser, W. H., and Pratt, D. T., "Thermodynamic Cycle Analysis of Pulse Detonation Engines," *Journal of Propulsion and Power*, Vol. 18, No. 1, 2002, pp. 68–76.

[2] Kaemming, T., "Integrated Vehicle Comparison of Turbo-Ramjet Engine and Pulsed Detonation Engine," *Journal of Engineering for Gas Turbines and Power*, Vol. 125, No. 1, 2003, pp. 257–262.

[3] Roy, G. D., Frolov, S. M., Borisov, A. A., and Netzer, D. W., "Pulse Detonation Propulsion: Challenges, Current Status, and Future Perspective," *Progress in Energy and Combustion Science*, Vol. 30, No. 6, 2004, pp. 545–672.

[4] Ma, L., Sanders, S. T., Jeffries, J. B., and Hanson, R. K., "Monitoring and Control of a Pulse Detonation Engine Using a Diode-Laser Fuel Concentration and Temperature Sensor," *Proceedings of the Combustion Institute*, Vol. 29, 2003, pp. 161–166.

[5] Tangirala, V. E., Dean, A. J., Chapin, D. M., Pinard, P. F., and Varatharajan, B., "Pulsed Detonation Engine Processes: Experiments and Simulations," *Combustion Science and Technology*, Vol. 176, No. 10, 2004, pp. 1779–1808.

[6] Brophy, C. M., Werner, S., and Sinibaldi, J. O., "Performance Characterization of a Valveless Pulse Detonation Engine," AIAA Paper 2003-1344, 2003.

[7] Nguyen, Q.-V., Mongia, R. K., and Dibble, R. W., "Real-Time Optical Fuel-to-Air Ratio Sensor for Gas Turbine Combustors," *Proceedings of SPIE—The International Society for Optical Engineering*, Vol. 3535, Jan. 1999, pp. 124–130.

[8] Tomita, E., Kawahara, N., Nishiyama, A., and Shigenaga, M., "In Situ Measurement of Hydrocarbon Fuel Concentration Near a Spark Plug in an Engine Cylinder Using the 3.392 mu m Infrared Laser Absorption Method: Application to an Actual Engine," *Measurement Science & Technology*, Vol. 14, No. 8, 2003, pp. 1357–1363.

[9] Hinckley, K. M., and Dean, A. J., "Time Resolved Measurements of Fuel-Air Stoichiometry in Pulse Detonation Engines Using a Non-Intrusive Laser Sensor," AIAA Paper 2005-0628, 2005.

[10] Sanders, S. T., Mattison, D. W., Muruganandam, T. M., and Hanson, R. K., "Multiplexed Diode-Laser Absorption Sensors for Aeropropulsion Flows," AIAA Paper 2001-0412, 2001.

[11] Klingbeil, A. E., Jeffries, J. B., and Hanson, R. K., "Temperature- and Pressure-Dependent Absorption Cross Sections of Gaseous Hydrocarbons at 3.39 μm," *Measurement Science & Technology*, Vol. 17, No. 7, 2006, pp. 1950–1957.

[12] Drallmeier, J. A., "Hydrocarbon Absorption Coefficients at the 3.39 mu m He-Ne Laser Transition," *Applied Optics*, Vol. 42, No. 6, 2003, pp. 979–982.

[13] Siegman, A. E., "Physical Properties of Gaussian Beams," *Lasers*, University Science Books, Sausalito, CA, 1986.

[14] Hecht, J., *Understanding Fiber Optics*, 3rd ed., Prentice–Hall, Upper Saddle River, NJ, 1999.

[15] Dereniak, E. L., and Boreman, G. D., *Infrared Detectors and Systems*, John Wiley & Sons, New York, 1996.

[16] Brophy, C. M., Sinibaldi, J. O., Ma, L., and Klingbeil, A. E., "Effects of Non-Uniform Mixture Distributions on Pulse Detonation Engine Performance," AIAA Paper 2005-1304, 2005, pp. 5103–5112.

[17] Tangirala, V. E., Dean, A. J., Pinard, P. F., and Varatharajan, B., "Investigations of Cycle Processes in a Pulsed Detonation Engine Operating on Fuel–Air Mixtures," *Proceedings of the Combustion Institute*, Vol. 30, No. 2, 2004, p. 2817.

[18] Klingbeil, A. E., Jeffries, J. B., and Hanson, R. K., "Tunable Mid-IR Laser Absorption Sensor for Time-Resolved Hydrocarbon Fuel Measurements," *Proceedings of the Combustion Institute*, Vol. 31, 2007, pp. 807–815.

N. Chokani
Associate Editor